An Efficient Method for Fast Simulation of Scanning Tunneling Microscopy with Tip Effect.

ARTICLE *in* THE JOURNAL OF PHYSICAL CHEMISTRY A · APRIL 2014

Impact Factor: 2.69 · DOI: 10.1021/jp5018218 · Source: PubMed

4 AUTHORS, INCLUDING:

Ruiqi Zhang

University of Science and Technology of China

5 PUBLICATIONS **11** CITATIONS

SEE PROFILE

Zhenpeng hu

Nankai University

39 PUBLICATIONS **771** CITATIONS

SEE PROFILE

Jinlong Yang

University of Science and Technology of China

510 PUBLICATIONS **11,085** CITATIONS

SEE PROFILE

THE JOURNAL OF PHYSICAL CHEMISTRY A

Article

pubs.acs.org/JPCA

Efficient Method for Fast Simulation of Scanning Tunneling Microscopy with a Tip Effect

Ruiqi Zhang,[†] Zhenpeng Hu,[§] Bin Li,*[,†,‡] and Jinlong Yang*[,†,‡]

[†]Hefei National Laboratory for Physics at Microscale and [‡]Synergetic Innovation Center of Quantum Information & Quantum Physics, University of Science and Technology of China, Hefei, Anhui 230026, China

[§]School of Physics, Nankai University, Tianjin 300071, China

ABSTRACT: On the basis of Bardeen's perturbation theory on electron tunneling and inspired by Paz et al.'s study, a new expression for the tunneling current between the scanning tunneling microscopy (STM) tip and sample has been obtained, and it provides us with an efficient method to simulate STM images. The method can be implemented in any code of first-principles computing software, which offers the wave functions of the tip and sample, calculated independently at the same footing, as input. By calculating the integral with fast Fourier transform (FFT), simulating the STM image of a given sample surface by a database of different tips on a PC turns out to be not a time-consuming work. Compared with Paz et al.'s method, our method abandons the application of the vacuum Green function and possesses better computing efficiency, fewer parameters, and more reasonable simulated results especially at lower computing cost. Simple tip−sample systems, such as H−H and Pd_2−Ag_2, are taken as benchmarks to test our method. The topographic images of a CO molecule adsorbed on a Cu(111) surface obtained by using a tungsten tip and a CO-terminated tip are also simulated, and the simulated results are in good agreement with the experimental ones.

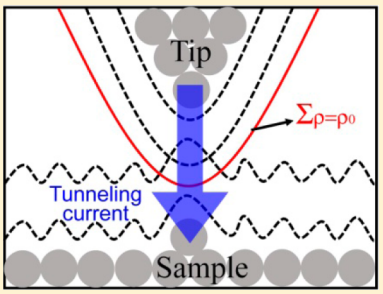

1. INTRODUCTION

Scanning tunneling microscopy (STM)[1−3] can produce atomic-resolution images of metal or semiconductor surfaces, and it has provided unprecedented knowledge about a rich variety of surface science aspects.[4] However, STM has a major drawback that it cannot give us a straightforward proper interpretation of a topographic image[5] because it is tightly related to the frontier orbitals of the sample. Fortunately, with the help of comparison between the results from first-principles theoretical simulations and the experimental data, a reasonable understanding of the STM data may be obtained. Many theoretical approaches thus have been brought up for explaining the experimental data.[6−11] Among these approaches, the ones based on Bardeen's perturbation theory (Bardeen's approach)[12,13] have been widely used, and as a simplified extension of Bardeen's approach, the Tersoff−Hamann (T−H) approximation[14,15] is the most popular model applied to understand the STM image. In the T−H approximation, the wave function of the STM tip is taken as an s-wave, and then, the tunneling current is proportional to the local density of states of the sample. Although the T−H approximation can give simulation results in qualitative agreement with some experiments, it is generally not so easy to attain quantitative data or to provide explanations to many experiments due to the simplification of the STM tip. For example, the T-H approximation failed in explaining the observed negative differential resistances[16−18] and STM images with chemically modified tips[19,20] because the s-wave tip model is not intended as an accurate description of the electronic structure of a real tip. Therefore, it is better to go back to the original Bardeen's approach to consider the impact of a real STM tip.

However, it is a time-consuming and cumbersome work to simulate the STM image using Bardeen's approach implemented with the traditional numerical integration method for tunneling matrix elements, which calls for us to perform different computations for different set positions of a tip relative to the sample. Paz et al. proposed a method (abbreviated as the Paz method) to simulate STM images in a single calculation, in which the Bardeen matrix elements are expressed in terms of convolutions.[21,22] Although their method is efficient, it has some disadvantages, and there is still room for improvement. In their method, the sample wave functions are propagated through the vacuum region, of which the effective electron potential is nearly flat, up to the proximities of the tip by means of the vacuum Green function, which brings the following problems: first, the calculation of the vacuum Green function needs additional parameters including the work-function-related κ and a Gaussian filtering parameter α,[22] so as to make their method tedious and affect the stability of simulated result; second, the assumption of a flat effective electron potential in the propagating region of the sample wave function is not solid enough in some cases so that a non-negligible computing error will emerge, and only the sample wave

Special Issue: International Conference on Theoretical and High Performance Computational Chemistry Symposium

Received: February 21, 2014
Revised: April 4, 2014
Published: April 7, 2014

dx.doi.org/10.1021/jp5018218 | J. Phys. Chem. A 2014, 118, 8953−8959

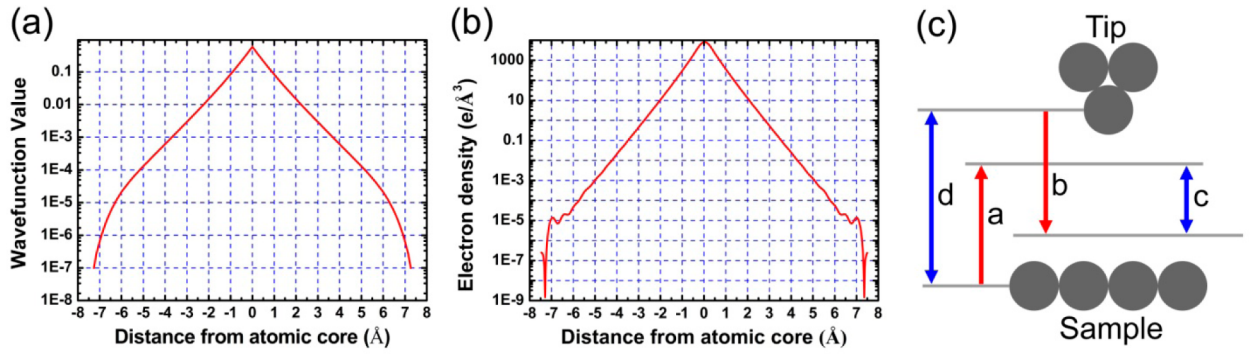

Figure 1. (a) The radial distributions of the H atom 1s orbital wave function calculated by the DMol3 package. (b) The radial distributions of the H atom 1s orbital electron density calculated by VASP. (c) A schematic view of the tip−sample system.

functions at the isosurface of one constant electron density ($\rho = \rho_0$) are taken into account, resulting in the calculation possibly being very sensitive to the selection of ρ_0 so as to bring instability to the result; at last, the calculation precision of the vacuum Green function also relies on the grid points of the wave function, meaning another source of computing errors.

Here, inspired by Paz et al.'s idea of expressing the Bardeen matrix elements in terms of convolutions, we have developed a new approach in calculating the tunneling matrix elements based on Bardeen's perturbation theory by selecting a unique separate surface between the tip and sample. In our method, the assumption that the sample wave function travels by means of the vacuum Green function is abandoned, and we adopt the reliable sample wave function calculated by the first-principles code; therefore, the additional parameters related to the vacuum Green function will not be considered, and then, some sources of computing errors and instabilities are eliminated. Fast Fourier transform (FFT) is used to reduce the computing time for the tunneling matrix, similar to the Paz method. The validity and efficiency of our developed method are exhibited by the tests using three tip−sample examples including an experimental system.

This paper is organized as follows. Our developed method is introduced in section 2. As a test and comparison, in subsection 3A, our method and the Paz method are applied in the same simple tip−sample system, that is, H−H, and it is shown that our method can give more reasonable results than the Paz method at lower computing cost. In order to test the practical applicability of our method, we also apply it to simulate the STM images of a simple tip−sample system Pd_2−Ag_2[6] in subsection 3B, and the topographic images of a CO molecule adsorbed on a Cu(111) surface[19] obtained by using a tungsten tip and a CO-terminated tip are given in subsection 3C. Subsection 3D presents a comparison of computing efficiencies of our method, the Paz method, and the traditional method. At last, a summary is presented in section 4.

2. THEORETICAL BASIS

The tunneling current by first-order perturbation theory is expressed as

$$I = \frac{2\pi e}{\hbar} \sum_{t,s} [f(\varepsilon_t) - f(\varepsilon_s)]|M_{ts}|^2 \delta(\varepsilon_t - \varepsilon_s + eV) \quad (1)$$

where $f(\varepsilon)$ is the Fermi distribution function, V is the applied voltage, ε is the energy of a certain state relative to the Fermi level, and subscripts t and s represent the tip and sample, respectively. M_{ts} is the tunneling matrix element between the tip state ψ_t and the sample state φ_s. The explicit formula for the tunneling matrix element is

$$\begin{aligned} M_{ts} &= M(\vec{r}_s, \vec{r}_t) \\ &= -\frac{\hbar^2}{2m} \int_\Sigma [\psi_t^*(\vec{r} - \vec{r}_t)\nabla\varphi_s(\vec{r} - \vec{r}_s) \\ &\quad - \varphi_s(\vec{r} - \vec{r}_s)\nabla\psi_t^*(\vec{r} - \vec{r}_t)]\, d\vec{S} \end{aligned} \quad (2)$$

where Σ represents a surface located in the vacuum region between the tip and the sample.

In the Paz method, the effective electron potential is thought to be nearly flat in the vacuum region at the distance larger than 5 Å from the sample; therefore, they proposed that the sample wave functions are propagated through the vacuum region by means of the vacuum Green function,[21,22] and the sample wave function at any point can be expressed as

$$\varphi_s(\vec{r}) = \int_\Sigma [G_t^*(\vec{r} - \vec{r}_s)\nabla\varphi_s(\vec{r}_s) - \varphi_s(\vec{r}_s)\nabla G_t^*(\vec{r} - \vec{r}_s)]\, d\vec{S} \quad (3)$$

The $G_t(\vec{r} - \vec{r}_s)$ is the vacuum Green function, which obeys $\nabla^2 G_t(\vec{r} - \vec{r}_s) - \kappa^2 G_t(\vec{r} - \vec{r}_s) = -\delta(\vec{r} - \vec{r}_s)$. On the basis of this assumption, M_{ts} is finally expressed in terms of convolutions.

In the Paz method, the vacuum Green function was used because they thought that it is technically difficult to obtain sufficiently accurate wave functions of both the tip and sample at the separate surfaces. However, in our view, the reliable wave function values of tip and sample states in the separation region of the tip−sample system can be obtained directly from the first-principles calculations. To validate our idea, we have made a test using the DMol3 package[23−25] with atomic orbitals bases. In the test, we examine the radial distributions of the H atom 1s orbital wave function, which is shown in Figure 1a. It is obvious that the wave function value calculated by DMol3 is reliable along the radial direction at the distance up to about 5.5 Å from the atomic core. We have also tested the radial distributions of the H atom 1s orbital electron density calculated by the Vienna ab initio simulation package (VASP)[26,27] with plane wave bases, and the result shown in Figure 1b also validates that at distances even up to about 6.0 Å from the atomic core, the wave function calculated by VASP is reliable.

Figure 1c presents a schematic view of the tip−sample system, in which d denotes the tip−sample distance from nucleus to nucleus and a and b represent the farthest distance at which we can still get reliable wave function values of the tip and sample states by the first-principles calculations,

dx.doi.org/10.1021/jp5018218 | J. Phys. Chem. A 2014, 118, 8953−8959

respectively. Because the normal tip−sample distance d is about 3−6 Å from nucleus to nucleus in actual experiments,[4] a and b values of at least 5.5 Å have already satisfied the requirement of computing the reliable M_{ts} at a separate surface. Even if the tip−sample distance d is enlarged to 8 Å, the region with reliable wave function values of both tip and sample states is still big enough ($c \approx 3$ Å in Figure 1c). Therefore, it is reasonable to adopt the sample wave function values calculated by first-principles calculations to compute M_{ts}, and the remaining task is to select a suitable separate surface Σ for the calculation of M_{ts}.

As a simplification of eq 2, the sample's position is set at the origin of the coordination system, and $\vec{r}_0$ represents the position of the tip relative to the sample, that is

$$\vec{r} = \vec{r} - \vec{r}_s \qquad \vec{r}_0 = \vec{r}_t - \vec{r}_s \tag{4}$$

We substitute the sample wave function $\varphi_s(\vec{r})$ calculated by first-principles calculations into eq 2, and then, M_{ts} will be expressed as

$$M_{ts} = -\frac{\hbar^2}{2m}\int_\Sigma [\psi_t^*(\vec{r} - \vec{r}_0)\nabla\varphi_s(\vec{r}) - \varphi_s(\vec{r})\nabla\psi_t^*(\vec{r} - \vec{r}_0)]\,d\vec{S} \tag{5}$$

Now, in fact, the main difference between our method and the Paz method is the way adopted to obtain a sample wave function on the separation surface, which leads to a different form of the tunneling matrix element M_{ts}.

In principle, any separation surface lying in the vacuum region between the two electrodes can be selected to calculate the integral, and a commonly used choice is a horizontal plane between the tip and sample (Figure 2a). Here, in order to utilize as much wave function information on the STM tip as we could take into account, we selected a surface with constant electron density (ρ_0) enveloping the tip (Figure 2b) as the separate surface Σ, which means

$$\rho_t(\vec{r})_{\vec{r}\in\Sigma} = \rho_0 \tag{6}$$

The equation of this surface could be written as

$$h_\Sigma(\vec{r}) = \log\left(\frac{\rho_t(\vec{r})}{\rho_0}\right) = 0 \tag{7}$$

Now, the tunneling matrix M_{ts} can be calculated as an integral in three-dimensional space with a confinement of eq 7

$$\begin{aligned} M_{ts} &= -\frac{\hbar^2}{2m}\int_\Sigma [\psi_t^*(\vec{r} - \vec{r}_0)\nabla\varphi_s(\vec{r}) - \varphi_s(\vec{r})\nabla\psi_t^*(\vec{r} - \vec{r}_0)]\,d\vec{S} \\ &= -\frac{\hbar^2}{2m}\int_\Sigma [\psi_t^*(\vec{r} - \vec{r}_0)\nabla\varphi_s(\vec{r}) - \varphi_s(\vec{r})\nabla\psi_t^*(\vec{r} - \vec{r}_0)]\cdot \\ &\quad \vec{n}_t(\vec{r} - \vec{r}_0)\,dS \\ &= -\frac{\hbar^2}{2m}\int [\psi_t^*(\vec{r} - \vec{r}_0)\nabla\varphi_s(\vec{r}) - \varphi_s(\vec{r})\nabla\psi_t^*(\vec{r} - \vec{r}_0)]\cdot \\ &\quad \vec{n}_t(\vec{r} - \vec{r}_0)\delta(h(\vec{r} - \vec{r}_0))\,dr^3 \\ &= -\frac{\hbar^2}{2m}\int [\vec{v}(\vec{r} - \vec{r}_0)\cdot\nabla\varphi_s(\vec{r}) - \varphi_s(\vec{r})u(\vec{r} - \vec{r}_0)]\,dr^3 \\ &= M_{ts}(\vec{r}_0) \end{aligned} \tag{8}$$

where $\vec{n}_t(\vec{r}) = \nabla\rho_t(\vec{r})/|\nabla\rho_t(\vec{r})|$ is the unit normal vector of surface Σ, $u(\vec{r} - \vec{r}_0) = \nabla\psi_t^*(\vec{r} - \vec{r}_0)\cdot\vec{n}_t(\vec{r} - \vec{r}_0)\delta(h(\vec{r} - \vec{r}_0))$ and $\vec{v}(\vec{r} - \vec{r}_0) = \psi_t^*(\vec{r} - \vec{r}_0)\vec{n}_t(\vec{r} - \vec{r}_0)\delta(h(\vec{r} - \vec{r}_0))$. Here, we use a Dirac delta function of h as a constraint to make the integration done on surface Σ.

From eq 8, one can see that M_{ts} is actually a function of $\vec{r}_0$ in a convolution form. It is well-known that Fourier transform can make the calculation of a convolution much easier. We thus calculate the M_{ts} in this way

$$\begin{aligned} M_{ts}(\vec{r}_0) &= F^{-1}[F[M_{ts}(\vec{r}_0)]] = F^{-1}[\tilde{M}_{ts}(\vec{k})] \\ &= -\frac{\hbar^2}{4m\pi}\int [\tilde{\vec{v}}(\vec{k})\cdot i\vec{k}\,\tilde{\varphi}_s(\vec{k}) - \tilde{\varphi}_s(\vec{k})\tilde{u}(\vec{k})]e^{i\vec{k}\cdot\vec{r}_0}\,dk^3 \end{aligned} \tag{9}$$

where $\tilde{\vec{v}}(\vec{k})$, $\tilde{\varphi}_s(\vec{k})$, and $\tilde{u}(\vec{k})$ are the Fourier transforms of $\vec{v}(\vec{r} - \vec{r}_0)$, $\varphi_s(\vec{r})$, and $u(\vec{r} - \vec{r}_0)$, respectively.

As a numerical implementation, $\varphi_s(\vec{r})$ and $\psi_t(\vec{r} - \vec{r}_0)$ are stored in three-dimensional grid boxes with the same footing, and the Dirac delta function in eq 8 is replaced by a Gaussian function with finite width. Then, for all positions of the tip with the same bias voltage, the M_{ts} will be evaluated through eq 8 in a single computation by using three-dimensional FFT. With the calculated M_{ts}, the STM topographic image and $I-V$ spectra can be easily obtained.

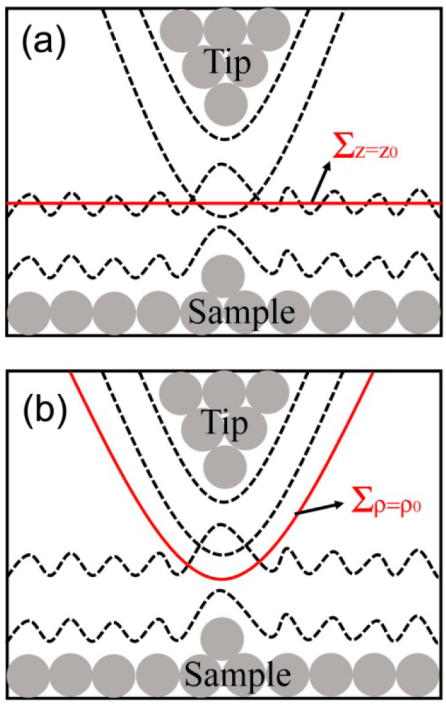

Figure 2. A schematic view of the tip wave functions and the sample wave functions having overlap in the vacuum region. The dashed lines represent the wave functions of sample or tip states. The solid red line represents the chosen separation surface used to calculate M_{ts}: (a) a horizontal plane between the tip and sample; (b) a specific surface with constant electron density enveloping the tip.

3. TESTS AND EXAMPLES

In this section, in order to check validity and efficiency of our method presented above, we apply it to three systems; the first one is the simplest theoretical model, in which both the tip and the sample are represented by only a hydrogen atom (H), so that we can make an explicit comparison between our method and the Paz method; the second one is a simple tip−sample

dx.doi.org/10.1021/jp5018218 | J. Phys. Chem. A 2014, 118, 8953−8959

system Pd_2−Ag_2, which was ever simulated using the molecular orbital model by Fujita et al.;[6] the last one is a CO molecule adsorbed on a Cu(111) surface, which was investigated in the STM experiment by Bartels et al.[19]

In our simulation, the electronic structure calculations are performed with the local density approximation (LDA)[28,29] implemented with the DMol3 package.[23−25] We choose the Vosko−Wilk−Nusair (VWN) local correlation functional[30] using parametrizations of Ceperley and Alder's electron gas Monte Carlo data.[31] The double numerical plus polarization basis set[23] and density functional semicore pseudopodtentials[25,32] are used. The self-consistent field procedure is carried out with a convergence criterion of 1.0×10^{-6} au on the electron density. Geometry optimizations are performed with convergence criteria of 5.0×10^{-3} au/Å on the gradient, 5.0×10^{-3} Å on the displacement, and 5.0×10^{-5} au on the energy.

A. H−H System. Both the tip and sample are modeled by a single H atom. The two atoms are set with a separation of 6.0 Å along the z direction in a box with 15.0 Å × 15.0 Å × 20.0 Å in three dimensions. The calculated contour maps of the tunneling matrix elements $|M_{ts}|^2$ between two H 1s orbitals with different parameters are shown in Figure 3. For test and

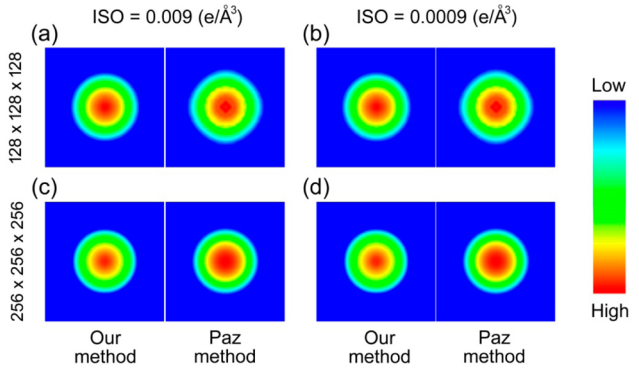

Figure 3. Contour maps of the tunneling matrix elements $|M_{ts}|^2$ for H−H system simulated by our method and the Paz method. For (a) and (c), the value of the constant electron density is set to be 0.009 e/Å^3; for (b) and (d), the value of the constant electron density is set to be 0.0009 e/Å^3. For (a) and (b), the number of sample points is 128 × 128 × 128; for (c) and (d), the number of sample points is 256 × 256 × 256.

comparison, two values of constant electron density (ρ_0 = 0.009 and 0.0009 e/Å^3) and the two numbers of sampling points (128 × 128 × 128 and 256 × 256 × 256) are used.

It is well-known that the isosurface of the wave function of the H 1s orbital is spherical; therefore, the contour maps of $|M_{ts}|^2$ should be circular. Obviously, as shown in Figure 3a and b, the results simulated by the Paz method are not accurate enough so that the circle pattern has a small distortion (diamond-like pattern). Only after the number of sampling points is further increased (such as 256 × 256 × 256), the almost perfect circle-like images are obtained by the Paz method, as shown in Figure 3c and d. This problem could be ascribed to the calculation related to vacuum Green function requesting enough dense sampling points. As a contrast, our simulation presents a proper image even when adopting sparser sampling points (128 × 128 × 128). On the other hand, the simulated results in Figure 3 also indicate that for both methods, the choice of ρ_0 has no sensitive influence on the qualitative pattern of the simulated STM image (actually, 0.00009 and 0.000009 e/Å^3 have been also tested, and the results change little). However, we find that for the real implementation, the Paz method should consider too many parameters, such as the work-function-related κ and the tricky Gaussian filtering function.[21,22] This results in a picky selection of those parameters to get a reasonable image, while on the contrary, our method is almost parameter-independent. All these may arise from the basic approximation in the Paz method that only the wave functions on a constant electron density surface ($\rho = \rho_0$) of both electrodes were propagated with the Green's function, which loses the precision in physics and makes the whole process complicated.

B. Pd_2−Ag_2 System. In this system, we use a metal dimer built by two Pd atoms as the model of the tip because it is the top atom of the tip that plays an important role in producing the tunneling current and the STM image,[4] which suggests that it is not a bad model using metal dimers as the tip. At the same time, a dimer built by two Ag atoms is chosen as the model of the sample. The geometrical structure of the Pd_2−Ag_2 system is shown in Figure 4a. We set these two metal dimers in a box,

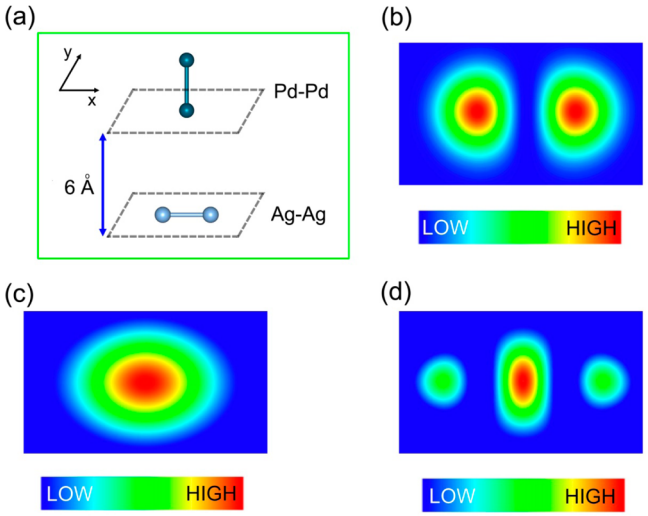

Figure 4. (a) Schematic view of the Pd_2−Ag_2 system. Silver−white balls and green balls represent Ag and Pd atoms, respectively. (b−d) Contour maps of the tunneling matrix elements; (b) is the one from the d_{z^2}-derived σ-antibonding orbital of Pd_2 to the s_{px}-derived σ-antibonding orbital of Ag_2; (c) is the one from the s-derived σ-bonding orbital of Pd_2 to the p_z-derived π-bonding orbital of Ag_2; and (d) is the one from the degenerate $d_{xz}(d_{yz})$-derived π-antibonding orbitals of Pd_2 to the s_{px}-derived σ-antibonding orbital of Ag_2.

which is 15.0 Å × 15.0 Å along the horizontal xy plane and 20.0 Å in the perpendicular z direction. As shown in Figure 4a, the tip is in the vertical plane, and the sample is in the horizontal plane, with the distance in the vertical direction between the tip and sample being set to 6.0 Å. The interatomic distances of the Ag−Ag and Pd−Pd dimers are chosen to be the experimental values of 2.89 and 2.75 Å, respectively.

The contour maps of the tunneling matrix elements $|M_{ts}|^2$ for three kinds of tunneling transitions are shown in Figure 4b−d. Figure 4b corresponds to the electron tunneling from the d_{z^2}-derived σ-antibonding orbital of Pd_2 to the s_{px}-derived σ-antibonding orbital of Ag_2; Figure 4c corresponds to the one from the s-derived σ-bonding orbital of Pd_2 to the distorted s-derived σ-bonding orbital of Ag_2; and Figure 4d corresponds to the ones from the degenerate $d_{xz}(d_{yz})$-derived π-antibonding

dx.doi.org/10.1021/jp5018218 | J. Phys. Chem. A 2014, 118, 8953−8959

orbitals of Pd_2 to the sp_x-derived σ-antibonding orbital of Ag_2. Here, we select the same molecular orbitals as those used in the study by Fujita et al.[6] As shown in Figure 4, our results successfully reproduce the analytical results, validating that our method is reasonable when dealing with different types of orbitals.

C. CO Chemisorbed on the Cu(111) Surface. In this simulation, the Cu(111) surface is modeled as a repeated slab geometry with four layers of copper, and a CO molecule is adsorbed at the on-top site and stands upright on the Cu(111) surface, which is in agreement with the experimental system explored by Bartels et al.[19] As shown in Figure 5a and b, our

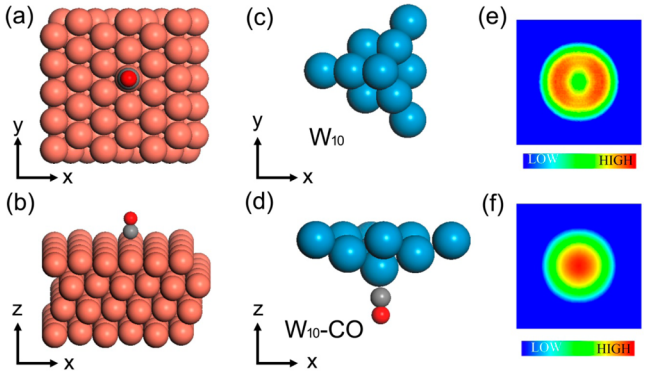

Figure 5. (a) Schematic top view of the CO molecule chemisorbed on the Cu(111) surface. (b) Schematic side view of the CO molecule chemisorbed on the Cu(111) surface. The dull-red balls, gray ball, and red ball represent copper, carbon, and oxygen atoms, respectively. (c) The top view of the W(111) bcc pyramid tip. (d) The side view of CO adsorbed on the W_{10} tip. The blue, gray, and red balls represent tungsten, carbon, and oxygen atoms, respectively. (e) The simulated STM topographic image obtained with a W_{10} tip with a sample bias of 1.0 V. (f) The simulated STM topographic image obtained with a W_{10}–CO tip with a sample bias of 1.0 V.

calculating model of the sample uses a 122 atom unit cell with periodic boundary conditions. We adopt a vacuum space in the z direction of about 15.0 Å, which is large enough to make sure that there is no interaction between periodic images of the sample. The optimized O–C/Cu–C bond lengths from our calculations are 1.15 and 1.83 Å, respectively. Two STM tips used in the experiment by Bartels et al.[19] are considered; the first tip is a tungsten bcc pyramid pointing in the (111) direction with 10 atoms (W_{10}); the second tip is a CO molecule adsorbed at the bottom of the W_{10} tip (W_{10}–CO). The optimized distance of the W–C and C–O bond lengths in the two tips are 2.00 and 1.17 Å, respectively. The geometries of the two tips are presented in Figure 5c and d.

Next, to compare with experiment directly, we performed STM image simulation by using our proposed method. The simulated constant height images of the CO molecule adsorbed on the Cu(111) surface obtained with W_{10} and W_{10}–CO tips are shown in Figure 5e and f, respectively. The sample bias is set to 1.0 V. As shown in Figure 5e, the CO molecule exhibits a pattern of depression surrounded by a protruding halo when it is imaged with a clean STM W tip. At the same time, the CO molecule presents itself as a protrusion (Figure 5f) when a W tip having a CO molecule at its apex is used. These simulated STM images coincide with the observed results in the experiment by Bartels et al.[19] It is ensured that the electron tunneling processes from the d_{z^2}-derived orbital of the W tip to the $p_x(p_y)$-derived π-antibonding orbitals of CO on a Cu surface and from the $p_x(p_y)$-derived π-antibonding orbitals of CO on a W tip to the same types of orbitals of CO on a Cu surface molecule are responsible for two images, the same as the conclusion by our previous study using the traditional real space integration method with pure cluster models.[33] Therefore, our proposed method is indeed applicable to simulate and interpret the real experimental cases with various types of orbitals participating in the electronic tunneling process.

D. Tests of Computing Efficiency. The efficiency test of our proposed method is performed using a CPU [Intel(R) Xeon(R) CPU E5420 @2.50 GHz]. As a comparison, the test results of the traditional real space integration method (trapezoidal integration) and the Paz method using the same CPU will also be listed. We chose the H–H system presented in subsection 3A for our test, and in the test, the following three sampling points are used: 64 × 64 × 64, 128 × 128 × 128, and 256 × 256 × 256. The test results are shown in Table 1.

Table 1. Results of Efficiency Tests of Three Methods Using the Same Processor PC (including I/O time)

	computing time (unit: s)		
number of sampling points	traditional method	Paz method	our method
64 × 64 × 64	3481.072	1.275	0.990 (78%)[a]
128 × 128 × 128	115964.706	11.388	8.674 (76%)[a]
256 × 256 × 256	4068708.319	97.910	75.839 (77%)[a]

[a]The ratios of the computing time of our method relative to the one of the Paz method.

Because both the Paz method and our method can obtain the tunneling matrix element $|M_{ts}|^2$ in one integral through FFT, they give very large improvements over the traditional method in the computing time, as expected. These two methods also have a lower scaling factor of the computing time relative to the number of sampling points compared to that of the traditional method.

As discussed before, the Paz method should compute more stuff than our method. Therefore, it is reasonable that our method can save at least 20% of time compared to the Paz method for the same computing purpose using the same sampling points and same CPU [Intel(R) Xeon(R) CPU E5420 @2.50 GHz] with the same optimized level of the compiler, as shown in Table 1. Furthermore, the code of our method can be converted to a Real-to-Real FFT rather than a Complex-to-Complex FFT technically, which would benefit the memory usage for a dense grid.

In the above tests, only the STM images are simulated, and we do not try to simulate the I–V spectra because the I–V spectra simulation cannot make use of the benefit of FFT that results in the fast simulation when using our method to simulate the STM images. Without any new approximation beyond the Bardeen's perturbation theory, our method should be also able to handle the I–V spectra simulation correctly, as shown by our previous studies using the traditional real space integration method.[18,34]

4. CONCLUSION

We have developed a new method for fast simulation of STM images based on Bardeen's perturbation theory and inspired by Paz et al.'s work[21,22] from first-principles calculations. This method makes the calculation of the tunneling matrix be

dx.doi.org/10.1021/jp5018218 | J. Phys. Chem. A 2014, 118, 8953–8959

performed in a convolution form, which provides a frame to use FFT. The wave functions of the tip and sample can be calculated independently at the same footing within density functional theory (or other first-principles methods). Three examples are tested by our method, and the simulated results are consistent with previously reported ones. Moreover, our method not only provide a great improvement of the computing efficiency over the traditional method because of implementing FFT, but it also has better efficiency, stability, and rationality of the result compared to the Paz method. Our method thus makes it possible to fast compare different tips' effect on STM and provides us a way to interpret STM experimental results in real time.

AUTHOR INFORMATION

Corresponding Authors

*E-mail: libin@mail.ustc.edu.cn. Phone: +86-551-63601747. Fax: +86-551-63603748 (B.L.).

*E-mail: jlyang@ustc.edu.cn. Phone: +86-551-63606408. Fax: +86-551-63603748 (J.Y.).

Author Contributions

The manuscript was written through contributions of all authors. All authors have given approval to the final version of the manuscript.

Notes

The authors declare no competing financial interest.

ACKNOWLEDGMENTS

This work is partially supported by the National Key Basic Research Program (2011CB921404), by NSFC (21121003, 91021004, 21233007, 21203099, 21273210), by CAS (XDB01020300), by the Doctoral Fund of Ministry of Education of China (20120031120033), by Fundamental Research Funds for the Central Universities, by the Research Program for Advanced and Applied Technology of Tianjin (13JCYBJC36800), and by USTCSCC, SCCAS, Tianjin, and Shanghai Supercomputer Centers.

REFERENCES

(1) Binnig, G.; Rohrer, H.; Gerber, C.; Weibel, E. Tunneling through a Controllable Vacuum Gap. *Appl. Phys. Lett.* **1982**, *40*, 178−180.

(2) Binnig, G.; Rohrer, H.; Gerber, C.; Weibel, E. 7 × 7 Reconstruction on Si(111) Resolved in Real Space. *Phys. Rev. Lett.* **1983**, *50*, 120−123.

(3) Binnig, G.; Rohrer, H. Scanning Tunneling Microscopy. *Surf. Sci.* **1983**, *126*, 236−244.

(4) Chen, C. J. *Introduction to Scanning Tunneling Microscopy*; Oxford University Press: New York, 1993.

(5) Magoga, M.; Archambault, F.; Cerdá, J. I. Nt_STM: A Step Forward in Scanning Tunneling Microscopy (STM) Simulations. *Comput. Phys. Commun.* **2012**, *183*, 1246−1249.

(6) Fujita, T.; Nakai, H.; Nakatsuji, H. Ab Initio Molecular Orbital Model of Scanning Tunneling Microscopy. *J. Chem. Phys.* **1996**, *104*, 2410−2417.

(7) Briggs, G. A. D.; Fisher, A. J. STM Experiment and Atomistic Modelling Hand in Hand: Individual Molecules on Semiconductor Surfaces. *Surf. Sci. Rep.* **1999**, *33*, 1−81.

(8) Büttiker, M.; Imry, Y.; Landauer, R.; Pinhas, S. Generalized Many-Channel Conductance Formula with Application to Small Rings. *Phys. Rev. B* **1985**, *31*, 6207−6215.

(9) Hofer, W. A. Challenges and Errors: Interpreting High Resolution Images in Scanning Tunneling Microscopy. *Prog. Surf. Sci.* **2003**, *71*, 147−183.

(10) Hofer, W. A.; Foster, A. S.; Shluger, A. L. Theories of Scanning Probe Microscopes at the Atomic Scale. *Rev. Mod. Phys.* **2003**, *75*, 1287−1331.

(11) Ness, H.; Fisher, A. J. Nonperturbative Evaluation of STM Tunneling Probabilities from Ab Initio Calculations. *Phys. Rev. B* **1997**, *56*, 12469−12481.

(12) Bardeen, J. Tunneling from a Many-Particle Point of View. *Phys. Rev. Lett.* **1961**, *6*, 57−59.

(13) Gottlieb, A. D.; Wesoloski, L. Bardeen's Tunnelling Theory as Applied to Scanning Tunnelling Microscopy: A Technical Guide to the Traditional Interpretation. *Nanotechnology* **2006**, *17*, R57−R65.

(14) Tersoff, J.; Hamann, D. R. Theory and Application for the Scanning Tunneling Microscope. *Phys. Rev. Lett.* **1983**, *50*, 1998−2001.

(15) Tersoff, J.; Hamann, D. R. Theory of Scanning Tunneling Microscope. *Phys. Rev. B* **1985**, *31*, 805−813.

(16) Zeng, C. G.; Wang, H. Q.; Wang, B.; Yang, J. L.; Hou, J. G. Negative Differential-Resistance Device Involving Two C_{60} Molecules. *Appl. Phys. Lett.* **2000**, *77*, 3595−3597.

(17) Blanco, J. M.; Flores, F.; Pérez, R. STM-Theory: Image Potential, Chemistry and Surface Relaxation. *Prog. Surf. Sci.* **2006**, *81*, 403−443.

(18) Chen, L.; Hu, Z. P.; Zhao, A. D.; Wang, B.; Luo, Y.; Yang, J.L.; Hou, J. G. Mechanism for Negative Differential Resistance in Molecular Electronic Devices: Local Orbital Symmetry Matching. *Phys. Rev. Lett.* **2007**, *99*, 146803.

(19) Bartels, L.; Meyer, G.; Rieder, K. H. Controlled Vertical Manipulation of Single CO Molecules with the Scanning Tunneling Microscope: A Route to Chemical Contrast. *Appl. Phys. Lett.* **1997**, *71*, 213−215.

(20) Hahn, J. R.; Lee, H. J.; Ho, W. Electronic Resonance and Symmetry in Single-Molecule Inelastic Electron Tunneling. *Phys. Rev. Lett.* **2000**, *85*, 1914−1917.

(21) Paz, Ó.; Brihuega, I.; Gómez-Rodríguez, J. M. Tip and Surface Determination from Experiments and Simulations of Scanning Tunneling Microscopy and Spectroscopy. *Phys. Rev. Lett.* **2005**, *94*, 056103.

(22) Paz, Ó.; Soler, J. M. Efficient and Reliable Method for the Simulation of Scanning Tunneling Images and Spectra with Local Basis Sets. *Phys. Status Solidi B* **2006**, *243*, 1080−1094.

(23) Delley, B. An All-Electron Numerical Method for Solving the Local Density Functional for Polyatomic Molecules. *J. Chem. Phys.* **1990**, *92*, 508−517.

(24) Delley, B. From Molecules to Solids with the $DMol^3$ Approach. *J. Chem. Phys.* **2000**, *113*, 7756−7764.

(25) Delley, B. Hardness Conserving Semilocal Pseudopotentials. *Phys. Rev. B* **2002**, *66*, 155125.

(26) Kresse, G.; Furthmüller, J. Efficient Iterative Schemes for Ab Initio Total-Energy Calculations Using a Plane-Wave Basis Set. *Phys. Rev. B* **1996**, *54*, 11169−11186.

(27) Kresse, G.; Furthmüler, J. Efficiency of Ab-Initio Total Energy Calculations for Metals and Semiconductors Using a Plane-Wave Basis Set. *Comput. Mater. Sci.* **1996**, *6*, 15−50.

(28) Kohn, W.; Sham, L. J. Self-Consistent Equations Including Exchange and Correlation Effects. *Phys. Rev.* **1965**, *140*, A1133−A1138.

(29) Sham, L. J.; Kohn, W. One-Particle Properties of an Inhomogeneous Interacting Electron Gas. *Phys. Rev.* **1966**, *145*, 561−567.

(30) Vosko, S. H.; Wilk, L.; Nusair, M. Accurate Spin-Dependent Electron Liquid Correlation Energies for Local Spin Density Calculations: A Critical Analysis. *Can. J. Phys.* **1980**, *58*, 1200−1211.

(31) Ceperley, D. M.; Alder, B. J. Ground State of the Electron Gas by a Stochastic Method. *Phys. Rev. Lett.* **1980**, *45*, 566−569.

(32) Hamann, D. R.; Schlüter, M.; Chiang, C. Norm-Conserving Pseudopotentials. *Phys. Rev. Lett.* **1979**, *43*, 1494−1497.

(33) Li, B.; Wang, H. Q.; Yang, J. L.; Hou, J. G. High-Resolution Scanning Tunneling Microscopy for Molecules. *Ultramicroscopy* **2004**, *98*, 317−334.

(34) Hu, Z. P.; Chen, L.; Zhao, A. D.; Li, Z. Y.; Wang, B.; Yang, J. L.; Hou, J. G. Detecting a Molecule−Surface Hybrid State by an Fe-Coated Tip with a Non-s-Like Orbital. *J. Phys. Chem. C* **2008**, *112*, 15603−15606.